3. Warren, W. S., Rabitz, H. & Dahleh, M. Coherent control of quantum dynamics: the dream is alive. *Science* **259,** 1581–1589 (1993).
4. Weiner, A. M. & Heritage, J. P. Picosecond and femtosecond Fourier pulse shape synthesis. *Rev. Phys. Appl.* **22,** 1619–1628 (1987).
5. Weiner, A. M., Leaird, D. E., Patel, J. S & Wullert, J. R. Programmable femtosecond pulse shaping by use of a multielement liquid-crystal phase modulator. *Opt. Lett.* **15,** 326–328 (1990).
6. Hillegas, C. W., Tull, J. X., Goswami, D., Strickland, D. & Warren, W. S. Femtosecond laser pulse shaping by use of microsecond radio-frequency pulses. *Opt. Lett.* **19,** 737–739 (1994).
7. Wefers, M. M. & Nelson, K. A. Generation of high-fidelity programmable ultrafast optical waveforms. *Opt. Lett.* **20,** 1047–1049 (1995).
8. Tannor, D. J. in *Molecules in Laser Fields* (ed. Bandrauk, A.) 403–446 (Dekker, New York, 1994).
9. Tannor, D. J. & Rice, S. A. Control of selectivity of chemical reaction via control of wave packet evolution. *J. Chem. Phys.* **83,** 5013–5018 (1985).
10. Tannor, D. J., Kosloff, R. & Rice, S. A. Coherent pulse sequence induced control of selectivity of reactions: exact quantum mechanical calculations. *J. Chem. Phys.* **85,** 5805–5820 (1986).
11. Shapiro, M. & Brumer, P. Laser control of product quantum state populations in unimolecular reactions. *J. Chem. Phys.* **84,** 4103–4104 (1986).
12. Tannor, D. J. & Rice, S. A. Coherence pulse sequence control of product formation in chemical reactions. *Adv. Chem. Phys.* **70,** 441–523 (1988).
13. Brumer, P. & Shapiro, M. Laser control of molecular processes. *Annu. Rev. Phys. Chem.* **43,** 257–282 (1992).
14. Potter, E., Herek, J. L., Pedresen, S., Liu, Q. & Zewail, A. H. Femtosecond laser control of a chemical-reaction. *Nature* **355,** 66–68 (1992).
15. Fourkas, J. T., Wilson, W. L., Wäckerle, G., Frost, A. E. & Fayer, M .D. Picosecond time-scale phase-related optical pulses: measurement of sodium optical coherence decay by observation of incoherent fluorescence. *J. Opt. Soc. Am. B* **6,** 1905–1910 (1989).
16. Heberle, A. P., Baumberg, J. J. & Köhler, K. Ultrafast coherent control and destruction of excitations in quantum wells. *Phys. Rev. Lett.* **75,** 2598–2601 (1995).
17. Salour, M. M. & Cohen-Tannoudji, C. Observation of Ramsey's interference fringes in the profile of doppler-free two-photon resonances. *Phys. Rev. Lett.* **38,** 757–760 (1997).
18. Teets, R., Eckstein, J. & Hänsch, T. W. Coherent two-photon excitation by multiple light pulses. *Phys. Rev. Lett.* **38,** 760–764 (1977).
19. Blanchet, V., Nicole, C., Bouchene, M. & Girard, B. Temporal coherent control in two-photon transitions: from optical interferences to quantum interferences. *Phys. Rev. Lett.* **78,** 2716–2719 (1997).
20. Bellini, M., Bartoli, A. & Hänsch, T. W. Two-photon Fourier spectroscopy with femtosecond light pulses. *Opt. Lett.* **22,** 540–542 (1997).
21. Judson, R. S. & Rabitz, H. Teaching lasers to control molecules. *Phys. Rev. Lett.* **68,** 1500–1503 (1992).
22. Meshulach, D., Yelin, D. & Silberberg, Y. Adaptive ultrashort pulse compression and shaping. *Opt. Commun.* **138,** 345–348 (1997).
23. Yelin, D., Meshulach, D. & Silberberg, Y. Adaptive femtosecond pulse compression. *Opt. Lett.* **22,** 1793–1795 (1997).
24. Meshulach, D., Yelin, D. & Silberberg, Y. Adaptive real-time femtosecond pulse shaping. *J. Opt. Soc. Am. B* **15,** 1615–1619 (1998).
25. Bardeen, C. J. *et al.* Feedback quantum control of molecular electronic population transfer. *Chem. Phys. Lett.* **280,** 151–158 (1997).

Acknowledgements. We thank C. Cohen-Tannoudji, N. Davidson, T. W. Hänsch and D. Tannor for helpful discussions, D. Yelin for his help in developing pulse-shaping techniques and A. Arie for loan of the Cs cell.

Correspondence and requests for materials should be addressed to Y.S. (e-mail: feyaron@wis.weizmann.ac.il).

Observation of a square flux-line lattice in the unconventional superconductor Sr_2RuO_4

T. M. Riseman*, P. G. Kealey*, E. M. Forgan*, A. P. Mackenzie*, L. M. Galvin*, A. W. Tyler*, S. L. Lee†, C. Ager†, D. McK. Paul‡, C. M. Aegerter§, R. Cubitt‖, Z. Q. Mao¶, T. Akima¶ & Y. Maeno¶

** School of Physics and Astronomy, University of Birmingham, Birmingham B15 2TT, UK*
† School of Physics and Astronomy, University of St Andrews, St Andrews KY16 9SS, UK
‡ Department of Physics, University of Warwick, Coventry CV4 7AL, UK
§ Physik-Institut der Universität Zürich, CH-8057, Zurich, Switzerland
‖ Institut Laue-Langevin, F-38042, Grenoble, France
¶ Department of Physics, Kyoto University, Kyoto 606-8052, Japan

The phenomenon of superconductivity continues to be of considerable scientific and practical interest. Underlying this phenomenon is the formation of electron pairs, which in conventional superconductors do not rotate about their centre of mass ('*s*-wave' pairing; refs 1, 2). This contrasts with the situation in high-temperature superconductors, where the electrons in a pair are believed to have two units of relative angular momentum ('*d*-wave' pairing; ref. 3 and references therein). Here we report small-angle neutron-scattering measurements of magnetic flux lines in the perovskite superconductor Sr_2RuO_4 (ref. 4), which is a candidate for another unconventional paired electron state—'*p*-wave' pairing, which has one unit of angular momentum[5–7]. We find that the magnetic flux lines form a square lattice over a wide range of fields and temperatures, which is the result predicted by a recent theory[8,9] of *p*-wave superconductivity in Sr_2RuO_4. This theory also indicates that only a fraction of the electrons are strongly paired and that the orientation of the square flux lattice relative to the crystal lattice will determine which parts of the three-sheet Fermi surface of this material are responsible for superconductivity. Our results suggest that superconductivity resides mainly on the 'γ' sheet[9].

Strontium ruthenate (SRO) has nearly two-dimensional metallic properties, with a well-established Fermi surface[10–13] consisting of three sheets (α, β, γ). Non-*s*-wave superconductivity in this material is implied by the strong suppression of the superconducting transition temperature (T_c) below its maximum value of ~1.5 K by non-magnetic impurities, which thus act as pair-breakers[7]. Noting that the γ-sheet of the SRO Fermi surface is mainly derived from different Ru orbitals than are the α- and β-sheets, Agterberg *et al.*[8] have argued that pairing interactions will only weakly couple the different orbitals. They propose that *p*-wave superconductivity will be primarily present on either the γ-sheet, or the α- and β-sheets, with weak superconductivity on the other. This argument has been recently extended by Agterberg[9], who has shown that the flux-line lattice (FLL) structure for field perpendicular to the RuO_2 planes is very likely to be square, and that the orientation of the square flux lattice relative to the crystal lattice indicates which sheet(s) of the Fermi surface are primarily responsible for superconductivity. Thus, by observations of the flux lattice, we can gain important information about superconductivity in this material.

Neutron-diffraction patterns were obtained from the FLL in a sample of SRO (see Methods). A contour plot of a typical result is

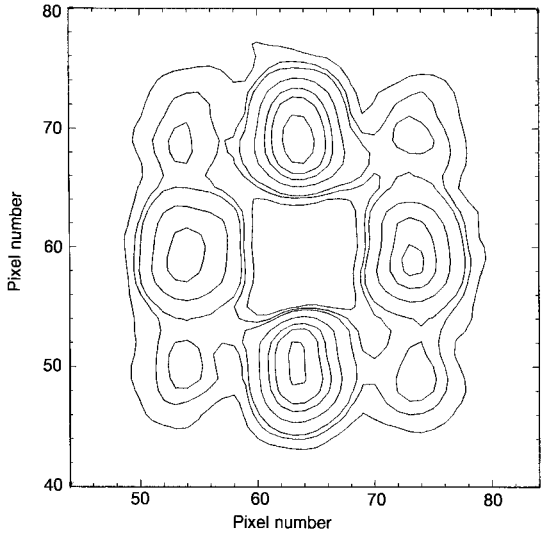

Figure 1 Contour plot of FLL diffraction pattern. With the geometry of our experiments, the diffracted neutrons form an image in the multidetector of the reciprocal lattice of the FLL: the central region of the detector has been masked. A field of 20 mT was applied parallel to **c** above T_c; data taken above T_c were subtracted from that obtained after cooling to 100 mK. The crystal **a** and **b** directions are horizontal and vertical in this figure. The sample shape causes the vertical spots to have different intensities from the horizontal ones, as discussed in Methods. The elongated shape of the spots reflects the shape of the exit aperture of the neutron guide.

shown in Fig. 1. The most notable feature of this pattern is that it is square, with the spots aligned with the **a**, **b** crystal axes, and that it certainly does not represent a triangular FLL. It should be noted that in addition to the $\{h,k\} = \{1,0\}$-type diffraction spots, higher-order {1,1} spots expected from a square FLL are observed in the expected positions; the intensity of the {1,1} spots is far too large for them to arise from multiple scattering. In Fig. 2, we show those regions of the B–T (magnetic induction-temperature) plane where we have established the existence of a square FLL in SRO; shortage of beamtime or weakness of the diffracted signal prevented a complete coverage of the relevant area of the plane, but we have no evidence of any departure from the square lattice structure. Of particular note is the result at 5 mT, which was obtained using an incident wavelength of 30 Å to detect the very long intervortex spacing of 0.64 μm. To our knowledge, this is the lowest-field FLL ever investigated by small-angle neutron scattering (SANS), and shows that there can be an overlap between this technique and decoration. A square FLL in SRO is also indicated by muon spin rotation (μSR) experiments in a purer sample than ours (G. M. Luke, personal communication), and in a less pure one[14]. The cumulative evidence of all these experiments is that in SRO a square FLL is widespread, and possibly intrinsic to its superconductivity.

It should be emphasised that with the field along the four-fold axis of the tetragonal structure of SRO, the original London or Ginzburg–Landau (GL) theories are necessarily isotropic[15], and hence predict a triangular rather than a square FLL. However, if non-local terms are added to the supercurrent response in the London theory[16], or higher-order gradient terms are added to the GL theory[17], then square FLLs can occur. Such theories tend to give a triangular flux lattice as T tends to T_c, where non-local effects become unimportant, and also at low magnetic inductions at all temperatures, because the response of any superconductor at long distances tends towards the London response. It appears that these approaches can explain the FLL transformations and square lattices seen in borocarbide superconductors in terms of Fermi surface anisotropy: see refs 17 and 18, and references therein. In general such effects are expected to be stronger in low-κ superconductors, which will have stronger interactions between the cores of adjacent flux lines. (The Ginzburg–Landau parameter is defined by $\kappa = \lambda/\xi$, where λ is the magnetic penetration depth and ξ is the coherence length.) It should also be noted that unconventional superconductivity is not necessarily implied by a square FLL: such a structure was also observed many years ago in a low-κ lead alloy[19]. However, another class of theories can also give rise to non-triangular lattices: these are extended GL theories, with more than one order parameter. For instance, d-wave superconductivity (with an s-wave component) in copper oxides is also expected to give rise to square FLLs[20]. Another example is the recent theory of p-wave superconductivity in SRO (ref. 9), which also leads to a square FLL. Using that theory (or indeed, a non-p-wave theory[16]), the relative orientation of the FLL and crystal lattice observed here implies that superconductivity in SRO resides principally in the γ-band electrons. This is not too surprising: we would expect this band to have the strongest pairing interaction, as it has the largest mass enhancement[13].

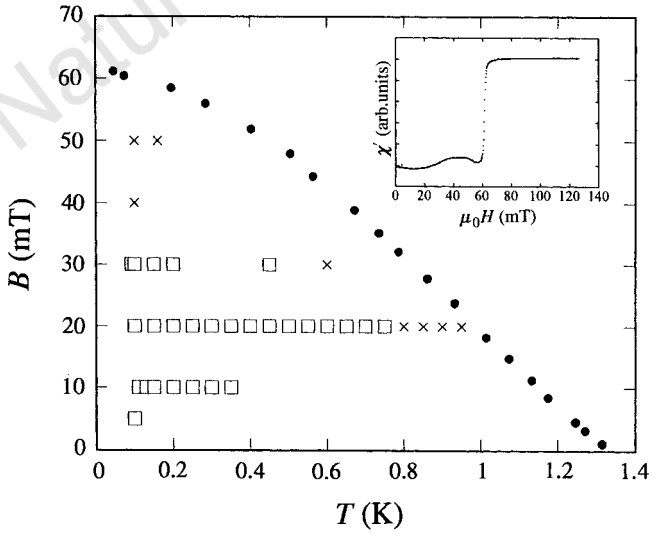

Figure 2 Observations in the B–T plane of a square FLL. By neutron scattering, a square FLL was observed at points marked with a square; at those marked with a cross, there was insufficient intensity to detect a FLL. The temperature dependence of B_{c2} for our sample with field parallel to **c** is also shown (filled circles). The transition was determined by measurement of the in-phase response of the a.c. susceptibility, χ'; a typical trace (at $T = 70$ mK) is shown as the inset.

To obtain further information about the properties of the superconductor, it is necessary to understand the intensity of the FLL signal, or equivalently, the magnitude of the Fourier components $|F_{hk}|$ of the magnetic field, described in Methods. In a high-κ superconductor, the London model is appropriate, and it gives $|F_{hk}|$ directly in terms of the temperature-dependent penetration depth, $\lambda(T)$, and hence the superfluid density, $n_S(T)$:

$$F_{hk}^{\text{London}} = \frac{B}{1 + q_{hk}^2\lambda^2(T)}, \quad \text{with } \frac{1}{\lambda^2(T)} \propto n_S(T) \tag{1}$$

Here $\mathbf{q}_{hk}$ are the reciprocal lattice wavevectors of the FLL. In a low-κ superconductor such as SRO, this will be modified by vortex core overlap. We choose to represent this by using the exact solution of the GL equations, calculated by the method of Brandt[21]. This gives $F_{hk}^{\text{GL}}/F_{hk}^{\text{London}}$ as a function $f(B/B_{c2})$, where f is weakly κ-dependent. In order to use this approach, we need the upper critical field B_{c2} (and the coherence length ξ from $B_{c2} = \Phi_0/2\pi\xi^2$, where Φ_0 is the flux quantum), which was determined as described in Methods and is plotted in Fig. 2.

Assuming the validity of the core overlap correction, we calculated a self-consistent set of λ and κ from the average integrated intensity of the horizontal spots. At 20 mT and 100 mK we obtain $\lambda = 194(16)$ nm and $\kappa = 2.6(2)$ ($f = 0.43$). Similar values have been obtained by μSR measurements (G. M. Luke, personal communication), and our value of κ is also supported by estimates of the critical field H_c from recent heat-capacity measurements on high-quality samples (S. NishiZaki and Y.M., unpublished data). The intensity of the weak {1,1} spots is difficult to separate from that of the {1,0} reflections, but appears to be somewhat larger than that given by the GL model with these parameters. We could not observe {2,0} reflections, and this is in accord with calculations of their expected intensity. It should be remembered that GL theory is only exact close to T_c and the calculations used a single-component order parameter, which may not be the case here. However, the mutual consistency of these results encourages us to believe that we have obtained reliable superconducting parameters for our sample.

We now compare our value of $B_{c2}(T = 0)$ with estimates from the Fermi surface properties, using the predictions of the BCS theory. With a cylindrical Fermi surface[22] for band i of radius k_F^i with carriers of effective mass $m = m_i^* m_e$, where m_e is the electron mass:

$$B_{c2}(0) = \frac{2\pi}{\gamma}\Phi_0\left(\frac{k_B T_c m_e}{\hbar^2}\right)^2\left(\frac{m_i^*}{k_F^i}\right)^2 \tag{2}$$

Here $\ln(\gamma)$ is Euler's constant (0.577); we note that this equation is slightly different from the standard BCS result, which is for a spherical Fermi surface. We have included a band index i as the Fermi surface in SRO consists of three bands. As suggested elsewhere[23], the value of $B_{c2}(0)$ in a multi-band superconductor will be controlled by the band giving the highest value. The calculated values are shown in Table 1, and it is clear that the γ-band is in surprisingly good agreement with our observations. These values strongly suggest that at least in high fields, the super-

Table 1 Fermi surface properties and superconducting parameters of Sr_2RuO_4

	α (holes)	β (electrons)	γ (electrons)
k_F^i (Å^{-1}) (ref. 10)	0.302(2)*	0.621(3)	0.750(4)
N_i (ref. 10)	0.216(2)	0.914(9)	1.334(13)
m_i^*	3.4(2)	7.5(4)	14.6(7)
m_i^*/k_F^i	11.3(6)	12.1(6)	19.5(10)
N_i/m_i^*	0.064(3)	0.122(6)	0.091(5)
$B_{c2}(0)$ (mT) Eq. (2)	19(2)	22(2)	58(6)
$\lambda_L(0)$ (nm) Eq. (3)	$\alpha+\beta+\gamma$: 98(2)†		
$\lambda_L(0)$ (nm)	$\alpha+\beta$: 120(3)		γ: 171(4)
λ_L (experiment)	194(16) nm: from SANS at 100 mK		
$B_{c2}(0)$ (experiment)	63 mT: from a.c. measurements		

Values of m_i^* are revised values from ref. 13.
* Error in last figure in parentheses.
† Value using all three bands and $V_M = 5.71 \times 10^{-5}$ m^3 (ref. 32).

conductivity of SRO is mainly due to the γ-band, because one would expect the other bands to be depaired at these fields. (However, it should be noted that more exotic pairing could alter the numerical factors in equation (2).)

We can also calculate the low-temperature value of the penetration depth λ(0) from the Fermi surface properties, and compare this with λ from the SANS results. The free-electron expression is: $1/\lambda^2(0) = ne^2\mu_0/m_e$, where n is the electron density. If there are several bands, this generalizes (for either spherical or cylindrical Fermi surfaces) to:

$$\frac{1}{\lambda^2(0)} = \frac{e^2\mu_0}{m_e}\sum_i \frac{n_i}{m_i^*} = \frac{N_A e^2 \mu_0}{V_M m_e}\sum_i \frac{N_i}{m_i^*} \qquad (3)$$

where N_i is the number of electrons per formula unit in band i and V_M/N_A is the volume of one formula unit. Table 1 shows the result of applying equation (3) to all three bands: the value of λ comes out much smaller than our low-temperature experimental value. Now λ represents the strength of Meissner screening at long distances, and it depends only on the response of the electronic charges to the magnetic vector potential **A**, and not on the nature of the pairing. It can be shown[24] that all parts of the Fermi surface that have a gap contribute to the low-temperature value of λ. It seems clear that reasonable agreement with our other results can only be obtained by assuming that under the conditions of our experiment only the γ-surface contributes significantly to λ.

All our results are consistent with ideas of orbital-dependent *p*-wave superconductivity[8,9]. Within that framework, a non-time-reversal-invariant superconducting state is expected[9], and has recently been observed[25]. We briefly discuss alternative schemes. One is a "non-unitary" pairing state[26,27], which also breaks time-reversal symmetry and can have nodes in the gap. However, such a state only occurs (as seen in the A1 phase of ^{3}He) if some extra stabilizing factor such as strong coupling is present[26]. Estimates of the coupling strength[28] make this state unlikely. We should also consider *d*-wave pairing: however, to break time-reversal symmetry all the way to T_c, one needs two degenerate states, and the only candidate (Γ_5^+ in the nomenclature of table IV in ref. 29) has nodes on the Fermi surface, where the *z*-component of the wavevector k_z is zero. Such a k_z-dependence of the gap is not expected in a two-dimensional material such as SRO. We conclude that the symmetry and orientation of the FLL and the values of the superconducting parameters all indicate that superconductivity in strontium ruthenate occurs primarily on the γ-sheet of the Fermi surface, and that the *p*-wave model[8,9] gives the most consistent explanation of our results as a whole. □

Methods

Sample preparation and properties. The sample of Sr_2RuO_4 was grown by the floating-zone technique with excess RuO_2 as a flux[30]. It formed a rod of approximately elliptical cross-section (2.5 × 3.5 mm), with the **c**-direction of the tetragonal structure (perpendicular to the RuO_2 planes) along the short axis of the ellipse, and one of the **a/b** directions ~30° from the axis of the rod. T_c was 1.28 K (mid-point) with width (10–90%) of ~60 mK, measured by low-frequency a.c. susceptibility. The highest T_c so far obtained in this material is 1.48 K, so our sample was subject to a small (~15%) depairing by the residual electron scattering.

SANS techniques. A length of 8 mm was diamond-cut from the growth rod; this was held mechanically, and by a small quantity of glue, to a copper plate, mounted on the mixing chamber of a dilution refrigerator. This was placed between the poles of an electromagnet with holes parallel to the field for transmission of neutrons. The magnetic field was parallel to the **c**-axis of the crystal within 0.5°, and the FLL was observed using long-wavelength neutrons, incident nearly parallel to the applied field, on instrument D22 at the Institut Laue Langevin. Typical wavelengths employed were 14 Å, with a spread (full-width at half-maximum) of 12%. Transmitted neutrons were registered at a 128 × 128 pixel multidetector (pixel size 7.5 × 7.5 mm) 17.71 m beyond the sample. The main beam was intercepted by a Cd beamstop and the weak diffracted beams due to the FLL were extracted from the background scattering from sample and cryostat by subtracting data taken above T_c.

Measurement of integrated intensity. Integrated intensities of FLL diffraction spots lying in the horizontal plane could be measured by rotating the electromagnet and the sample together about a vertical axis, rocking these spots through the Bragg condition. The integrated intensity I_{hk} of a (h, k) reflection with wavevector q_{hk} may be related to a Fourier component F_{hk} of the magnetic field variation inside the FLL, via the relationship: $I_{hk} = 2\pi\phi(\mu/4)^2(V\lambda_n^2/\Phi_0^2 q_{hk})|F_{hk}|^2$, where ϕ is the incident flux of neutrons of wavelength λ_n, V is the sample volume, Φ_0 is the flux quantum and μ is the neutron magnetic moment in nuclear magnetons. In initial measurements, we formed the FLL by cooling the sample in constant applied field. This gave a rather broad rocking-curve width of several degrees, which reduced the peak intensity and made the integration for I_{hk} inaccurate. We suspect that the width was due to random pinning and bending of the flux lines into a non-optimum configuration (the large anisotropy of SRO will make the flux lines particularly easy to bend). In $NbSe_2$, another anisotropic superconductor, the quality of the FLL under such circumstances was improved by passing a current[31]. We therefore induced currents in our sample by oscillating the applied field by ±1 mT at ~0.5 Hz during cooling. This increased the peak diffracted intensity by a factor ~2 and the rocking-curve width was reduced to ~1.5° half-width at half-maximum (the integrated intensity should be unchanged). The diffraction pattern shown in Fig. 1 was observed after cooling in this manner. The rocking-curve width was still large compared with the Bragg θ for all the diffracted spots, so the complete pattern is seen with the incident neutron beam parallel to the field. It will be noted that the vertical spots are ~1.6 times more intense than the horizontal spots: we believe that this is because with a (nearly vertical) rod-shaped sample, most residual flux-line bending will be in the horizontal direction.

Measurement of B_{c2}. This was determined from the a.c. susceptibility (0.2 mT at 97 Hz applied parallel to **c**) of a small piece cut from the growth rod immediately adjacent to the SANS sample, as a function of temperature and magnetic field B applied parallel to the crystal **c**-axis. A typical in-phase response as a function of magnetic field (swept up or down) at constant temperature is shown in Fig. 2 inset. At low levels of excitation the flux lines are pinned, so a strong diamagnetic response is seen as soon as the sample enters the mixed state from the normal state. B_{c2} is taken as the mid-point of the a.c. transition.

Received 25 June; accepted 18 August 1998.

1. Bardeen, J., Cooper, L. N. & Schrieffer, J. R. Theory of superconductivity. *Phys. Rev.* **108,** 1175–1204 (1957).
2. Anderson, P. W. & Morel, P. Generalised Bardeen-Cooper-Schrieffer states and the proposed low temperature phase of liquid He^3. *Phys. Rev.* **123,** 1911–1934 (1961).
3. Tsuei, C. C. & Kirtley, J. R. Phase-sensitive tests of pairing symmetry in cuprate superconductors. *Physica C* **282,** 4–11 (1997).
4. Maeno, Y. *et al.* Superconductivity in a layered perovskite without copper. *Nature* **372,** 532–534 (1994).
5. Rice, T. M. & Sigrist, M. Sr_2RuO_4: an electronic analogue of ^{3}He? *J. Phys: Condens. Matter* **7,** L643–648 (1995).
6. Maeno, Y. Electronic states of the superconductor Sr_2RuO_4. *Physica C* **282-7,** 206–209 (1997).
7. Mackenzie, A. P. *et al.* Extremely strong dependence of superconductivity on disorder in Sr_2RuO_4. *Phys. Rev. Lett.* **80,** 161–164 & (erratum) 3890 (1998).

8. Agterberg, D. F., Rice, T. M. & Sigrist, M. Orbital dependent superconductivity in Sr_2RuO_4. *Phys. Rev. Lett.* **78,** 3374–3377 (1997).
9. Agterberg, D. F. Vortex lattice structures of Sr_2RuO_4. *Phys. Rev. Lett.* **80,** 5184–5187 (1998).
10. Mackenzie, A. P. *et al.* Quantum oscillations in the layered perovskite superconductor Sr_2RuO_4. *Phys. Rev. Lett.* **76,** 3786–3789 (1996).
11. Maeno, Y. & Yoshida, K. Fermi liquid properties and superconductivity of Sr_2RuO_4. *Czech. J. Phys.* **46,** Suppl. S6, 3097–3104 (1996).
12. Maeno, Y. *et al.* Two-dimensional Fermi liquid behavior of the superconductor Sr_2RuO_4. *J. Phys. Soc. Jpn* **66,** 1405–1408 (1997).
13. Mackenzie, A. P. *et al.* Fermi surface topography of Sr_2RuO_4. *J. Phys. Soc. Jpn* **67,** 385–388 (1998).
14. Aegerter, C. M. *et al.* Evidence for a square vortex lattice in Sr_2RuO_4 by muon-spin rotation measurements. *J. Phys: Condens. Matter* **10,** 7445–7451 (1998).
15. Hohenberg, P. C. & Werthamer, N. R. Anisotropy and temperature dependence of the upper critical field of type-II superconductors. *Phys. Rev.* **153,** 493–497 (1967).
16. Kogan, V. G. *et al.* Vortex lattice transitions in borocarbides. *Phys. Rev. B* **55,** 8693–8696 (1997).
17. De Wilde, Y. *et al.* The superconducting energy gap and vortex lattice structure in $LuNi_2B_2C$. *Physica C* **282-7,** 355–358 (1997).
18. Paul, D. McK. *et al.* Nonlocal effects and vortex lattice transitions in YNi_2B_2C. *Phys. Rev. Lett.* **80,** 1517–1520 (1998).
19. Obst, B. Rectangular flux line lattice in type II superconductors. *Phys. Lett A* **28,** 662–663 (1969).
20. Berlinsky, A. J., Fetter, A. L., Franz, M., Kallin, C. & Soininen, P. I. Ginzburg-Landau theory of vortices in d-wave superconductors. *Phys. Rev. Lett.* **75,** 2200–2203 (1995).
21. Brandt, E. H. Precision Ginzburg-Landau solution of ideal vortex lattices for any induction and symmetry. *Phys. Rev. Lett.* **78,** 2208–2211 (1997).
22. Schofield, A. J. Upper critical-field in the gauge-model. *Phys. Rev. B* **51,** 11733–11738 (1995).
23. Mackenzie, A. P. *et al.* Calculation of thermodynamic and transport-properties of Sr_2RuO_4 at low-temperatures using known Fermi-surface parameters. *Physica C* **263,** 510–515 (1996).
24. Rickayzen, G. in *Superconductivity* (ed. Parks, R. D.) 91 (Dekker, New York, 1969).
25. Luke, G. M. *et al.* Time-reversal symmetry breaking superconductivity in Sr_2RuO_4. *Nature* **394,** 558–561 (1998).
26. Sigrist, M. & Zhitomirsky, M. E. Pairing symmetry of the superconductor Sr_2RuO_4. *J. Phys. Soc. Jpn* **65,** 3452–3455 (1996).
27. Machida, K., Ozaki, M. & Ohmi, T. Odd-parity pairing superconductivity under tetragonal symmetry—possible application to Sr_2RuO_4. *J. Phys. Soc. Jpn* **65,** 3720–3723 (1996).
28. Mazin, I. I. & Singh, D. Ferromagnetic spin fluctuation induced superconductivity in Sr_2RuO_4. *Phys. Rev. Lett.* **79,** 733–736 (1997).
29. Sigrist, M. & Ueda, K. Phenomenological theory of unconventional superconductivity. *Rev. Mod. Phys.* **63,** 239–311 (1991).
30. Maeno, Y., NishiZaki, S., Yoshida, K., Ikeda, S. & Fujita, T. Normal-state and superconducting properties of Sr_2RuO_4. *J. Low. Temp. Phys.* **105,** 1577–1588 (1996).
31. Yaron, U. *et al.* Structural evidence for a 2-step process in the depinning of the superconducting flux-line-lattice. *Nature* **376,** 753–755 (1996).
32. Chmaissem, O., Jorgensen, J. D., Shaked, H., Ikeda, S. & Maeno, Y. Thermal expansion and compressibility of Sr_2RuO_4. *Phys. Rev. B* **57,** 5067–5070 (1998).

Acknowledgements. We thank J.-L. Ragazzoni of the ILL for setting up the dilution refrigerator, D. F. Agterberg for useful discussions, E. H. Brandt for giving us a copy of his program and G. M. Luke for communicating results before publication. One of us (A.P.M.) acknowledges the support of the Royal Society. This work was supported by the UK EPSRC, and CREST of Japan Science and Technology Corporation. The neutron scattering was carried out at the Institut Laue-Langevin, Grenoble.

Correspondence and requests for materials should be addressed to T.M.R. (e-mail: tmr@th.ph.bham.ac.uk).

Surface-promoted replication and exponential amplification of DNA analogues

A. Luther, R. Brandsch & G. von Kiedrowski

Lehrstuhl für Bioorganische Chemie, Ruhr-Universität Bochum, Universitätstrasse 150, NC 2/173, D-44780 Bochum, Germany

Self-replicating chemical systems have been designed and studied to identify the minimal requirements for molecular replication[1], to translate the principle into synthetic supramolecular systems[2] and to derive a better understanding of the scope and limitations of self-organization processes[3] that are believed to be relevant to the origin of life on Earth[4]. Current implementations make use of oligonucleotide analogues[5–12], peptides[13–17], and other molecules[18–24] as templates and are based either on autocatalytic, cross-catalytic, or collectively catalytic pathways for template formation. A common problem of these systems is product inhibition, leading to parabolic instead of exponential amplification[25]. The latter is the dynamic prerequisite for selection in the darwinian sense[26,27]. We here describe an iterative, stepwise procedure for chemical replication which permits an exponential increase in the concentration of oligonucleotide analogues. The procedure employs the surface of a solid support and is called SPREAD (surface-promoted replication and exponential amplification of DNA analogues). Copies are synthesized from precursor fragments by chemical ligation on immobilized templates, and then liberated and immobilized to become new templates. The process is repeated iteratively. The role of the support is to separate complementary templates which would form stable duplexes in solution. SPREAD combines the advantages of solid-phase chemistry with chemical replication, and can be further developed for the non-enzymatic and enzymatic amplification of RNA, peptides and other templates as well as for studies of *in vitro* evolution and competition in artificial chemical systems. Similar processes may also have played a role in the origin of life on Earth, because the earliest replication systems may have proliferated by spreading on mineral surfaces[28–33].

Stepwise 'feeding' procedures were previously employed in two different chemical systems that were reported as models of potentially prebiotic processes[10,34,35]. Li and Nicolaou achieved chemical replication of duplex DNA composed of palindromic (symmetrical) homopyrimidine and homopurine strands[10]. The homopyrimidine strand was synthesized from its precursor fragments via triple helix ligation, and then served as a template for the chemical ligation of the precursors of the homopurine strand. Thus, stepwise feeding with homopyrimidine and homopurine fragments prevented fragment complexation and therefore allowed switching between the respective triplex and duplex ligation intermediates. Ferris *et al.* have demonstrated the synthesis of long oligonucleotide- and peptide-like materials on the surface of mineral supports[34,35]. In these systems, stepwise feeding enabled the replenishment of activated precursors, and thus overcame the length-limiting effect of precursor hydrolysis. The conjunction of the above approaches, stepwise chemical replication and solid-phase chemistry, forms the basis of our procedure (Fig. 1).

For a demonstration of SPREAD (Fig. 2), two complementary 14-meric templates, **X** and **Y**, as well as four template fragments, $\mathbf{A}^x$, $\mathbf{B}^x$, $\mathbf{A}^y$ and $\mathbf{B}^y$, were synthesized using standard phosphoramidite chemistry. A thiol-modified support was obtained from

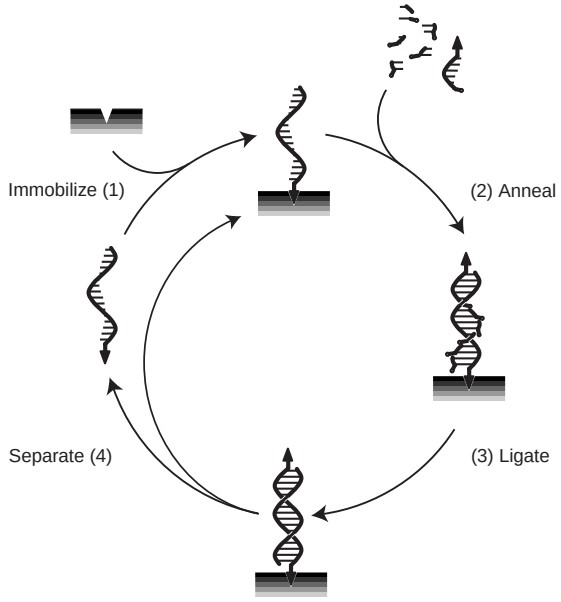

Figure 1 General scheme of the SPREAD procedure. (1) A template is immobilized by an irreversible reaction with the surface of a solid support. (2) The template binds complementary fragments from solution. (3) The fragments are linked together by chemical ligation. (4) The copy is released, and re-immobilized at another part of the solid support to become a template for the next cycle of steps. Irreversible immobilization of template molecules is thus a means to overcome product inhibition.